The $C_4H_4^{\bullet+}$ Potential Energy Surface. 2. The Jahn−Teller Stabilization of Ionized Tetrahedrane and Its Rearrangement to Cyclobutadiene Radical Cation[†,1]

Vojtěch Hrouda[‡] and Thomas Bally*

Institute of Physical Chemistry, University of Fribourg, Pérolles, CH-1700 Fribourg, Switzerland

Petr Čársky and Pavel Jungwirth

J. Heyrovský Institute of Physical Chemistry, Academy of Sciences of the Czech Republic, Dolejškova 3, 182 23 Prague 8, Czech Republic

Received: July 29, 1996; In Final Form: December 16, 1996[⊗]

The Jahn−Teller potential energy surface of the radical cation of tetrahedrane is explored by quantum chemical calculations and modeled analytically. The first- and second-order vibronic constants are evaluated. The rearrangement to the cyclobutadiene radical cation, which was previously predicted to occur with no activation, is investigated by the same quantum chemical method (CCSD(T)/cc-pVTZ//QCISD/6-31G*). It is shown that the localization of the HOMO which is necessary for adiabatic crossover requires some energy, which leads to a 0 K activation barrier of 4.3 kcal/mol for the process. It is concluded that the radical cations of substituted tetrahedranes should persist at low temperatures if they can be formed with little excess energy.

1. Introduction

Tetrahedrane (TH), the hydrocarbon incarnation of the simplest of the platonic solids, is also the most extravagant one.[2] We owe it to the perseverance of Prof. Maier and co-workers that some derivatives of this most strained of all known hydrocarbons have become available[3] and that hopes to make the parent compound remain alive, although this elusive goal has not been achieved to date.[4]

In particular, the suprisingly stable tetra-*tert*-butyl derivative (TH-tBu_4), which retains the high symmetry of the parent structure to the greatest extent,[5] has been subjected to detailed structural, spectroscopic, and chemical investigations.[2] Interestingly, TH-tBu_4 undergoes only three types of chemical reactions, i.e., thermal and photochemical rearrangement to the more stable cyclobutadiene derivative (CB-tBu_4), protonation, and oxidation. The present report focuses on the last of these, i.e., the fate of TH on ionization which according to all available experimental evidence leads to spontaneous rearrangement to $CB^{\bullet+}$.

Thus, it was found that upon chemical oxidation in CH_2Cl_2 at −70 °C, TH-tBu_4 gives ESR and ENDOR spectra indistinguishable from those obtained under the same conditions from CB-tBu_4.[6] On the other hand, electrochemical oxidation of TH-tBu_4 in acetonitrile was irreversible up to a scan rate of 10 V s^{-1} at −78 °C, and the reduction wave showed reversible reduction of the radical cation of CB-tBu_4 at 0.15 ± 0.10 V.[7] Moreover, it was shown that all products of oxidation reactions involving TH-tBu_4 arise from CB-$tBu_4^{\bullet+}$.[8] All of this indicates that the rearrangement of TH-$tBu_4^{\bullet+}$ to CB-$tBu_4^{\bullet+}$ is essentially activationless. This conclusion found support in MNDO calculations on $TH^{\bullet+}$ [7] and TH-$Me_4^{\bullet+}$ [6] which predicted spontaneous collapse of the strained tetrahedranes to cyclobutadienes on ionization.

However, the MNDO method is not a very fortunate choice for modeling this particular reaction as it absurdly overestimates the stability of four-membered relative to three-membered rings.[9]

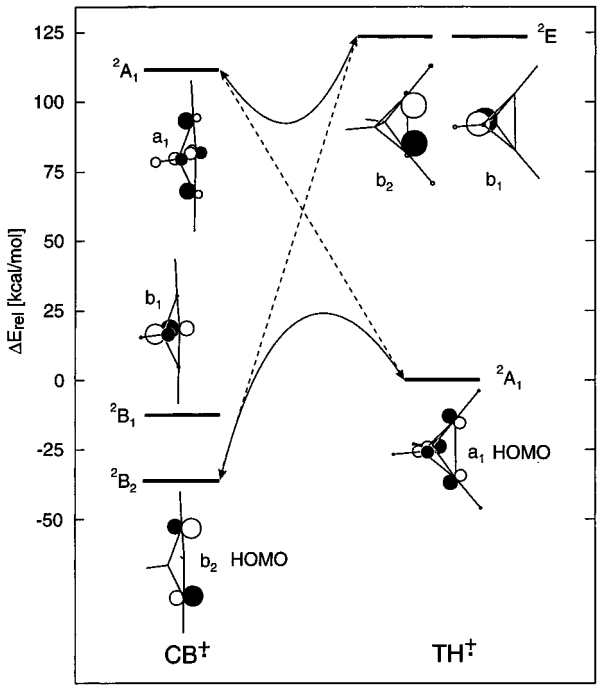

Figure 1. State correlation diagram and frontier MOs for the interconversion of $TH^{\bullet+}$ and $CB^{\bullet+}$. The equilibrium structures of the two isomers and the relative energies of the different states at these geometries are from ROHF/6-31G* calculations. The MOs of $TH^{\bullet+}$ are labeled within the C_{2v} symmetry shared by both isomers.

In addition the $TH^{\bullet+} \rightarrow CB^{\bullet+}$ rearrangement involves a crossing of the $^2A_1$ state of $TH^{\bullet+}$ and the $^2B_2$ state of (rhombic) $CB^{\bullet+}$ within the maximal C_{2v} symmetry shared by both compounds,[6] as illustrated by the correlation diagram in Figure 1. To avoid this crossing, the system must lose most of its symmetry,[6] and this entails a localization of spin and charge which is expected to be associated with an increase in energy.

Therefore, a completely barrierless interconversion appeared quite improbable to us, and we decided to reinvestigate this reaction as part of our ongoing studies of C_4 hydrocarbon radical cations,[10] using state-of-the-art theoretical methods. We begin

† Dedicated to Prof. Günter Maier on the occasion of his 65th birthday.
‡ On leave from the J. Heyrovský Institute of Physical Chemistry, Academy of Sciences of the Czech Republic, Prague, Czech Republic.
⊗ Abstract published in *Advance ACS Abstracts,* February 15, 1997.

S1089-5639(96)02287-6 CCC: $14.00

with an analysis of the Jahn−Teller distortions of $TH^{\bullet+}$ which turn out to provide substantial structural progress along the reaction coordinate leading to $CB^{\bullet+}$ and then continue to explore the region of the state crossing which contains the transition state for the title reaction.

2. Jahn−Teller Surface for a Tetrahedral System in a Doubly Degenerate Electronic State

Any nuclear configuration of a highly symmetrical molecule in a degenerate electronic state is unstable according to the Jahn−Teller (JT) theorem and tends to relax to a structure of lower symmetry in which this degeneracy is broken. Initially this distortion occurs along certain non-totally symmetric normal modes (often the components of a degenerate one), but as the relaxation proceeds, second-order effects may lead to significant deviations from those. In particular, geometry optimizations along the symmetry-breaking modes do not necessarily lead to stationary points on the potential energy surface, and reoptimization usually leads to further stabilization. The energy decrease is often driven by a decrease in nuclear repulsion which is zero in the first order (but nonzero in higher orders) of a perturbation series as one proceeds along non-totally symmetric normal modes.[11]

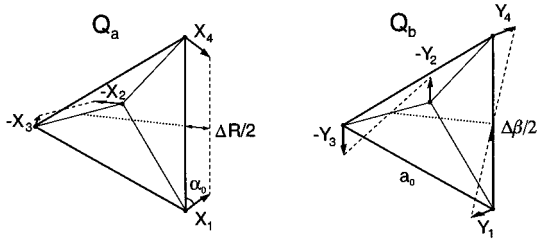

Figure 2. Jahn−Teller coordinates Q_a and Q_b expressed in a system of local Cartesian coordinates attached to each corner of a tetrahedron (the Z_i axes point toward the center of the tetrahedron). R is the distance between the midpoints of the C_1-C_4 and C_2-C_3 bonds, β stands for the angle of rotation of the two bonds around the line passing through these two midpoints, and a_0 is the C−C bond length in tetrahedrane.

Nevertheless it is useful to discuss JT surfaces in terms of analytic expressions which describe the vibronic interaction, such as they appear for example in Bersuker's book.[12] For the present case of a doubly degenerate ground state in T_d symmetry,[13] JT stabilization occurs along two orthogonal components of a normal mode of e-symmetry.[12] In the coordinate system shown in Figure 2, a symmetrized pair of such components can be assigned to a pair of coordinates Q_a and Q_b:

$$Q_a = {}^1/_2(X_1 + X_4 - X_2 - X_3)$$

$$Q_b = {}^1/_2(Y_1 + Y_4 - Y_2 - Y_3) \qquad (1)$$

where X_i and Y_i are 0 for a tetrahedral structure. In these coordinates and in a harmonic approximation, the expressions for the corresponding cross sections through the potential energy hypersurface (called "sheets" by Bersuker)[12] are

$$\epsilon_1 = {}^1/_2K_E(Q_a{}^2 + Q_b{}^2) + \epsilon_1^v(Q_a,Q_b)$$

$$\epsilon_2 = {}^1/_2K_E(Q_a{}^2 + Q_b{}^2) + \epsilon_2^v(Q_a,Q_b) \qquad (2)$$

where K_E is the force constant in the absence of vibronic coupling, whereas ϵ_1^v and ϵ_2^v are the roots of the vibronic secular equation

$$\begin{vmatrix} W_{11}^v - \epsilon^v & W_{12}^v \\ W_{21}^v & W_{22}^v - \epsilon^v \end{vmatrix} = 0 \qquad (3)$$

In the above determinant, the $W_{ij}^v(Q_a,Q_b)$ are the matrix elements $\langle\psi_i|\mathbf{W}^v|\psi_j\rangle$ of the vibronic Hamiltonian $\mathbf{W}^v$ over the two components ψ_i and ψ_j of the degenerate electronic state. We define the first- and second-order vibronic constants F_E and G_E as

$$F_E = \left\langle \psi_1 \left| \left(\frac{\partial V}{\partial Q_a}\right)_0 \right| \psi_1 \right\rangle, \qquad G_E = \frac{1}{2}\left\langle \psi_1 \left| \left(\frac{\partial^2 V}{\partial Q_a\,\partial Q_b}\right)_0 \right| \psi_2 \right\rangle \qquad (4)$$

where V is the energy due to interaction of the electrons with the nuclei and internuclear repulsion. If only the linear and quadratic terms of a perturbation series are taken into account, then eq 3 can be solved analytically[12,14] to yield

$$\epsilon_\pm^v = \pm[F_E{}^2(Q_a{}^2 + Q_b{}^2) + G_E{}^2(Q_a{}^2 + Q_b{}^2)^2 + 2F_EG_E(Q_a{}^3 - 3Q_aQ_b{}^2)]^{1/2} \qquad (5)$$

These solutions can be substituted for ϵ_1^v and ϵ_2^v in eqs 2 for the JT surfaces ϵ_1 and ϵ_2 which can therefore also be expressed analytically in Q_a and Q_b if the JT parameters K_E, F_E, and G_E are known. In the present study we will only be concerned with the lower "sheet" of the JT potential energy surface which is described by $\epsilon_1(Q_a,Q_b)$, using the minus sign in eq 5, and ignore the excited-state cone described by ϵ_2.

If the second-order vibronic constant G_E is zero, then ϵ_1 describes a rotationally invariant or "sombrero"-type surface.[15] The effect of nonzero G_E is to "warp" the bottom of the potential such as to introduce three equivalent minima and associated transition states, respectively, one pair of which is always located on the Q_a axis (if the product $F_E{\cdot}G_E$ is positive, $Q_a > 0$ for the minimum and $Q_a < 0$ for the transition state, and vice versa).

The potential surface $\epsilon_1(Q_a,Q_b)$ can be characterized by two energy-related parameters, the JT stabilization energy E_{JT} and the energy barrier $E^\ddagger$ between the minima. In terms of the quantities K_E, F_E, and G_E these two parameters can be expressed as[12]

$$E_{JT} = \frac{F_E{}^2}{2(K_E - 2|G_E|)} \qquad E^\ddagger = \frac{4E_{JT}|G_E|}{(K_E + 2|G_E|)} \qquad (6)$$

To evaluate K_E, $|F_E|$, and $|G_E|$ we need another relation which can be provided by a third, geometry-related parameter expressing for example the distance ΔQ_m of the JT minimum from the conical intersection of ϵ_1 and ϵ_2 along the Q_a axis:[16]

$$\Delta Q_m = |F_E|/(K_E - 2|G_E|) \qquad (7)$$

Actually, it turns out that the adiabatic potential of tetrahedral systems can be more conveniently expressed in a system of coordinates describing changes Δ in the distance (R) and the dihedral angle (β), respectively, between opposite sides of the tetrahedron, as shown in Figure 2 (note that these are linearly related to Q_a and Q_b for small displacements Δ):

$$\Delta R = \sin(\alpha_0){\cdot}Q_a$$

$$\Delta\beta \approx \tan(\Delta\beta) = (2/a_0){\cdot}Q_b \qquad (8)$$

where a_0 is the length of a side and α_0 the angle between that and a connected vector X_i [α_0 is given by symmetry, $\sin(\alpha_0) = 0.8165$]. These coordinates have the advantage that they convey a clear topological meaning and lend themselves well for the

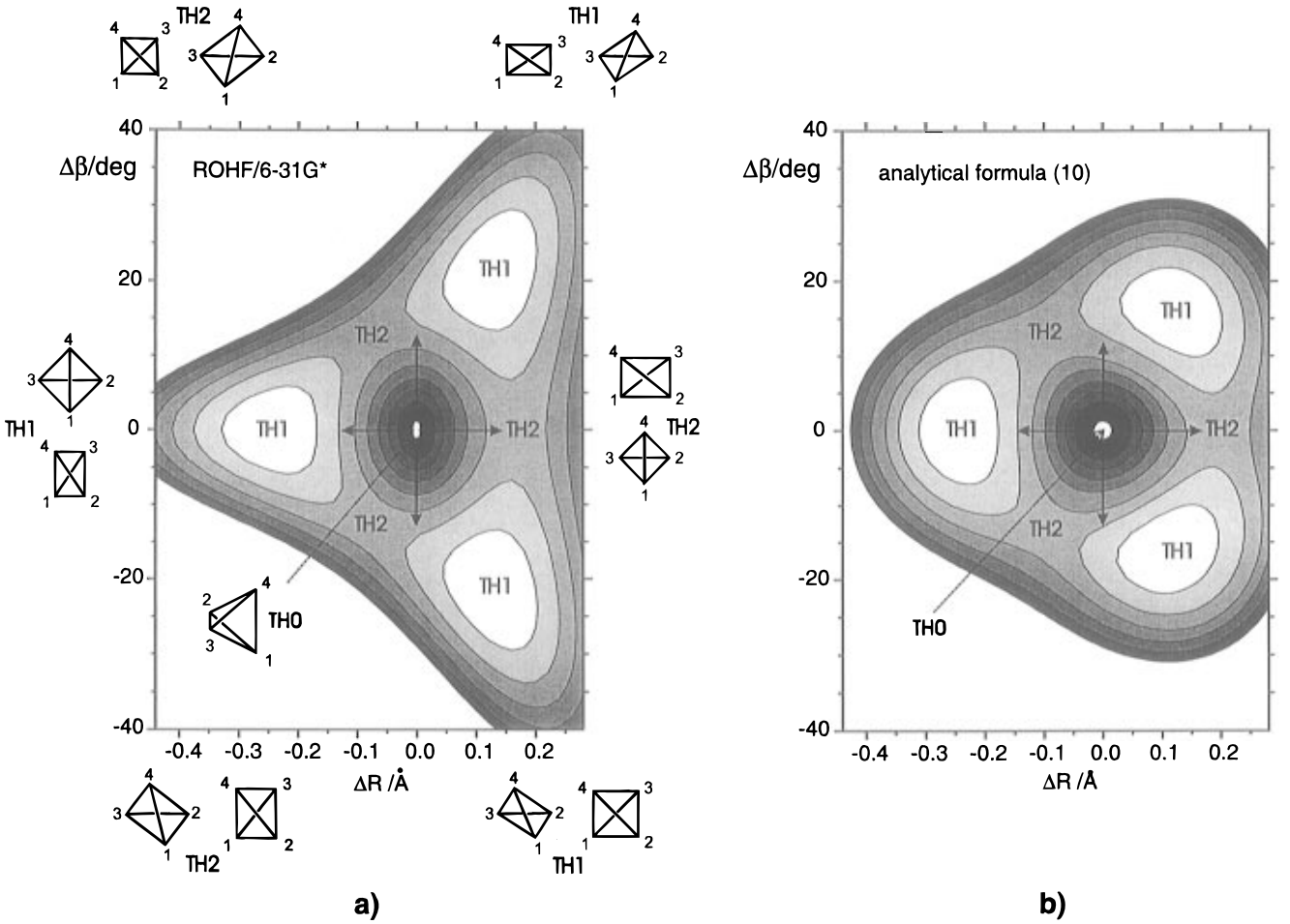

Figure 3. ΔR vs $\Delta\beta$ contour maps of the JT potential energy surface of $TH^{\bullet+}$ as obtained (a) from ROHF/6-31G* calculations, with all other parameters relaxed and (b) from the analytical expression 10 with the JT parameters K_E, $|F_E|$, and $|G_E|$ as obtained from the same calculations (cf. Table 2). The drawings around plot (a) show projections of the two triads of structures TH1 (minima) and TH2 (transition states) along two of the three C_2 axes (discussion see text).

construction of **Z** matrices. Thus we replace ΔQ_m in eq 7 by

$$\Delta R_m = \frac{\sin(\alpha_o)\cdot|F_E|}{(K_E - 2|G_E|)} \tag{9}$$

We will use eqs 6 and 9 to evaluate the JT parameters K_E, $|F_E|$, and $|G_E|$ from E_{JT}, $E^{\ddagger}$, and ΔR_m as obtained from quantum chemically calculated JT surfaces, and we will plot ϵ_1 as a function of ΔR and $\Delta\beta$, as obtained from eqs 2, 5, and 8:

$$\epsilon_1 = {}^1/_2 K_E(\Delta R^2 + \Delta\beta^2) - [F_E{}^2(\Delta R^2 + \Delta\beta^2) + G_E{}^2(\Delta R^2 + \Delta\beta^2)^2 + 2F_E G_E(\Delta R^3 - 3\Delta R\Delta\beta^2)]^{1/2} \tag{10}$$

However, before going into this we wish to point out a very elegant and convenient way to analyze the group theoretical features of JT surfaces, i.e., the *epikernel principle* introduced by Ceulemans and Vanquickenborne:[17] If G is the parent point group of a molecule, then the *kernel* $K(G,\Gamma)$ of a given irreducible representation Γ of G is the subgroup of G which contains all symmetry elements represented by the unit matrices in Γ. On the other hand, the *epikernel* $E(G,\Gamma)$ represents the subgroup of G containing all symmetry elements for which at least one basis function of Γ can be chosen to be invariant.

In our case $G = T_d$ and $\Gamma = e$, and it can be deduced[17] from the above definitions that $K(T_d,e) = D_2$ and $E(T_d,e) = D_{2d}$. The epikernel principle then states that (i) stationary points on the JT surface prefer epikernels to kernels, (ii) they prefer epikernels of the highest possible symmetry, and (iii) stable minima possess structures of maximal epikernel symmetry.[17] Thus, the epikernel principle predicts that the stationary points on the JT surface of $TH^{\bullet+}$ will be of D_{2d} rather than D_2 symmetry, as the calculations presented below also showed.

3. Computational Methods

Initially, all structures considered in this study were optimized at the restricted open-shell Hartree−Fock (ROHF) level (we did not use UHF to avoid possible problems with spin contamination). Subsequently, they were reoptimized by the UB3LYP density functional method[18] which has recently proven to give excellent agreement with experiment and higher level calculations for geometries and vibrational frequencies[19] and whose spin unrestricted variant is much less plagued by spin contamination than HF calculations.[20] For validation purposes, we also reoptimized all structures and characterized the resulting stationary points at the UQCISD level,[21] but, as expected, the geometries and frequencies turned out to be very similar to those obtained by B3LYP. All the above calculations were done with the standard 6-31G* basis set of Hariharan and Pople.[22]

To ascertain that single-determinant reference wave functions give a qualitatively correct description of the electronic structures of our $C_4H_4{}^{\bullet+}$ species, i.e., that strong nondynamic correlation effects which would require multideterminantal reference wave functions are absent, we performed (7,8)CASSCF calculations.[23] These showed in all cases that the reference configuration was over 93% and that no excited configuration contributed more than 1.5% (with the exception of rhombic $CB^{\bullet+}$ where the

TABLE 1: Energies (ΔE) and 0 K Internal Energies ($\Delta E_0 = \Delta E + \Delta$ZPE) in kcal/mol of $C_4H_4^{\bullet+}$ Structures[a] Relative to Ground-State $TH^{\bullet+}$ (TH1)

$C_4H_4^{\bullet+}$ structure	ROHF/6-31G*		UB3LYP/6-31G*		UQCISD/6-31G*		UCCSD(T)/cc-pVTZ[b]	
	ΔE	ΔE_0	ΔE	ΔE_0	ΔE	ΔE_0	ΔE	ΔE_0
TH0[c]	26.49		24.82		25.07		24.35	
TH2	5.52	4.96	5.64	5.20	5.62	5.08	4.88	4.35
TS	4.90	4.30	4.30	4.01	3.76	3.41	4.61	4.26
CB-rh	−36.12[d]	−37.39	−29.24	−28.26	−31.47	−30.43	−28.22	−27.18
CB-re	−38.80	−37.00	−31.35	−29.55	−30.71	−29.49	−29.82	−28.60
TH1 E [e]	−153.348 76		−154.353 82		−153.862 64		−154.053 40	
TH1 ZPE [f]	40.25		37.21		37.68		(37.68)	

[a] For B3LYP and QCISD optimized structures see Figure 4. TH2 and TS are transition states, TH1 and the two CB structures are minima at all levels, except where noted. [b] Single-point calculations at QCISD geometries; ΔZPE taken from vibrational analysis at the QCISD level. [c] At the geometry of neutral TH. Not a stationary point of $TH^{\bullet+}$, therefore no ΔE_0 given. [d] Transition state in ROHF.[1] [e] Total energies in hartree. [f] Zero-point vibrational energies in kcal/mol. In the ΔE_0 columns, the relative ZPEs are added to ΔE.

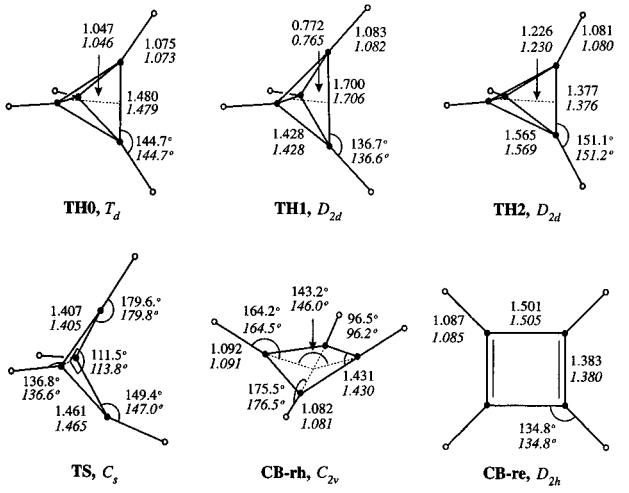

Figure 4. Geometries of stationary points on the $C_4H_4^{\bullet+}$ potential energy surface (TH0 is for neutral TH)[27] as obtained at the QCISD (normal) and B3LYP levels (italic), both with the 6-31G* basis set. TH2 and TS are saddle points, all other structures correspond to energy minima.

largest contribution was 2.4%). This proved that the single-reference-based QCISD[21] or CCSD[24] approaches to evaluate the dynamic correlation energy would be valid. On the basis of this, single-point energies were evaluated at the UCCSD(T) level[24] using Dunning's correlation-consistent triple-ζ (cc-pVTZ) basis set,[25] which gave 176 basis functions for C_4H_4. Zero-point energies (ZPE) for the evaluation of internal energy changes at 0 K, $\Delta E_0 = \Delta E + \Delta$ZPE were taken from the QCISD/6-31G* calculations.

All calculations were carried out with the Gaussian 94 suite of programs[26] on an SGI Power Challenge server, with the exception of the CCSD(T)/cc-pVTZ jobs which were run on a NEC SX3 vector machine.

4. Results and Discussion

4.1. Jahn−Teller Surface of $TH^{\bullet+}$. All features of the JT surface of $TH^{\bullet+}$ were evaluated in the framework of the coordinates ΔR and $\Delta\beta$ introduced in section 2. A contour map of the ROHF surface in these coordinates is shown in Figure 3a and will serve as a basis for the discussion of the higher-level results. In essence, there are three relevant types of structures (cf. Figure 4): (i) $TH^{\bullet+}$ in T_d symmetry (denoted TH0 in Figure 3) which is also the point of the conical intersection on the JT surface of $TH^{\bullet+}$.[27] (ii) The three equivalent minima ($^2A_1$ states in D_{2d} symmetry, TH1 in Figure 3) which are characterized by four short and two long C−C bonds (1.428 and 1.700 Å, respectively, at the QCISD level).

TABLE 2: Parameters for the JT Adiabatic Potential of $TH^{\bullet+}$ [a]

parameter	ROHF 6-31G*	UB3LYP 6-31G*	UQCISD 6-31G*	UCCSD(T) cc-pVTZ[b]
E_{JT}	26.49	24.82	25.07	24.35
$E^{\ddagger}$	5.52	5.64	5.62	4.88
ΔR_m	0.245	0.281	0.275	0.275
K_E	6.60	4.82	5.04	4.81
$\lvert F_E\rvert$	1.76	1.44	1.45	1.44
$\lvert G_E\rvert$	0.38	0.31	0.32	0.27

[a] E_{JT} and $E^{\ddagger}$ are in kcal mol^{-1}, ΔR_m is in Å, $|F_E|$ is in 10^2 kcal mol^{-1} Å^{-1}, and K_E and $|G_E|$ are in 10^2 kcal mol^{-1} Å^{-2}.

(iii) The three equivalent transition states ($^2B_1$ states in D_{2d}, TH2 in Figure 3) with four long and two short bonds (1.565 and 1.377 Å, respectively, by QCISD).

An interesting feature of the two sets of stationary points (which is unique to the T_d/e case) is that, although the structures in each set are geometrically and energetically identical, they are distinct in a topological sense: if the geometry of $TH^{\bullet+}$ is optimized along the R coordinate (cf. Figure 2), then structures TH1 and TH2 are attained strictly within D_{2d} symmetry. Conversely, if the optimization proceeds initially along the orthogonal coordinate β (i.e., keeping $\Delta R = 0$), then the symmetry descends to D_2 as β deviates from 90° ($\Delta\beta \neq 0$), but eventually the optimization converges again to TH1 or TH2, i.e., to structures of D_{2d} symmetry.

This is of course what is required by the epikernel principle (see above), but it does not become immediately evident, because the D_{2d} structures obtained along β differ from those which lie on R by the orientation of the coordinate system. Whereas in the latter, the S_4 axis connects the midpoints between C_2-C_3 and the C_1-C_4 bonds, it goes through the midpoints of the C_3-C_4 and the C_1-C_2 bonds for $\Delta\beta > 0$ (and through the midpoints of C_2-C_4 and C_1-C_3 for $\Delta\beta < 0$). We have tried to illustrate this feature by providing projections along two of the three axes in the little drawings which surround the potential energy surface in Figure 3a. These also allow us to see how the system "rotates" along the minimal energy path which connects the three minima TH1 via the three transition states TH2.

Table 1 lists the energies of TH0, TH1, and TH2 as obtained by geometry optimizations within T_d/D_{2d} symmetry with the ROHF, B3LYP, and QCISD methods, both with the 6-31G* basis set, and the results of the single-point CCSD(T) calculations with the larger cc-pVTZ basis set. From these we can obtain the three JT parameters E_{JT}, $E^{\ddagger}$, and ΔR_m which can in turn be used to evaluate K_E, $|F_E|$, and $|G_E|$. The compilation of these values in Table 2 shows that they do not depend very critically on the method, except perhaps for the simple ROHF/6-31G* level which gives values for K_E, $|F_E|$, and $|G_E|$ which

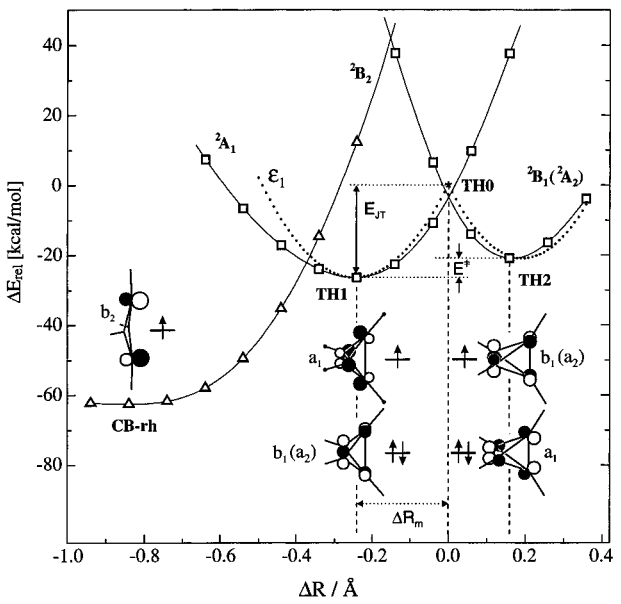

Figure 5. D_{2d} cross section of the JT surface of $TH^{\bullet+}$ (open squares)[28] and C_{2v} curve for the puckering of $CB^{\bullet+}$ (open triangles) from ROHF/6-31G* geometry optimizations for different values of the coordinate ΔR. The dotted line represents the curve according to eq 10, with the JT parameters K_E, $|F_E|$, and $|G_E|$ as obtained from the indicated ROHF values for ΔR_m, E_{JT}, and $E^\ddagger$ via eqs 6 and 9. Note that the $^2B_1$ state of $TH^{\bullet+}$ correlates with a $^2A_2$ state of $CB^{\bullet+}$ in C_{2v} symmetry (labels in parentheses refer to C_{2v}).

are 20−35% higher than those obtained at the correlated levels. Conversely, we note the excellent performance of the comparatively economic B3LYP model which gives results in close agreement with the much more expensive coupled cluster calculations.

With $E^\ddagger$ being as small as ≈5 kcal/mol, it is to be expected that the motion of $TH^{\bullet+}$ along the bottom of the JT surface will be very rapid, i.e., the JT distortion will be *dynamic*. The low $E^\ddagger$ may also have repercussions on experimental spectra (e.g., tunneling splitting of vibrational energy levels), but the study of such effects is beyond the scope and goals of the present article.

Obviously, in the case of $TH^{\bullet+}$, one of the minima TH1 lies at negative values of the ΔR coordinate, therefore the product $F_E \cdot G_E$ must have a negative sign (see the discussion above). With this additional piece of information we calculated the surface $\epsilon_1(\Delta R,\Delta\beta)$ by eq 10. An equipotential diagram of the lower sheet as obtained with the parameters from the ROHF/6-31G* calculation is shown in Figure 3b whereas a two-dimensional D_{2d} cross section along the ΔR coordinate is plotted in Figure 5. This includes also the ground state ($^2B_2$) surface of the product, $CB^{\bullet+}$, for the discussion in the following section. Apart from a wrong asymptotic behavior for large negative values of ΔR and large values of $\Delta\beta$ which is due to the harmonic approximation inherent in the model, the qualitative and quantitative agreement between parts a and b in Figure 3 is evident.[28]

4.2. Rearrangement of $TH^{\bullet+}$ to $CB^{\bullet+}$. As seen above, JT distortion of $TH^{\bullet+}$ leads to minima where one pair of opposite tetrahedral bonds have moved closer. As it happens, this is precisely what is required for the interconversion to $CB^{\bullet+}$, and hence one can say that the JT distortion results in *structural progress* along the reaction coordinate which connects the two isomers, in close analogy to the recently discussed case of the cyclooctateraene radical cation which relaxes to a [3.3.0]-bicyclic species upon excitation into a degenerate excited state.[29] However, in contrast to that case, significant changes in the wave function are required for $TH^{\bullet+}$ to cross over onto the $CB^{\bullet+}$ ground-state surface (cf. Figure 1). In particular, the HOMO of $TH^{\bullet+}$ at the TH1 minimum is symmetric with respect to a C_2 axis coinciding with the S_4 axis, whereas that of (rhombic) $CB^{\bullet+}$ is antisymmetric. A change of sign is only possible if a complete localization of the HOMO (and hence most of the spin) on one C−H unit occurs at some point along the reaction

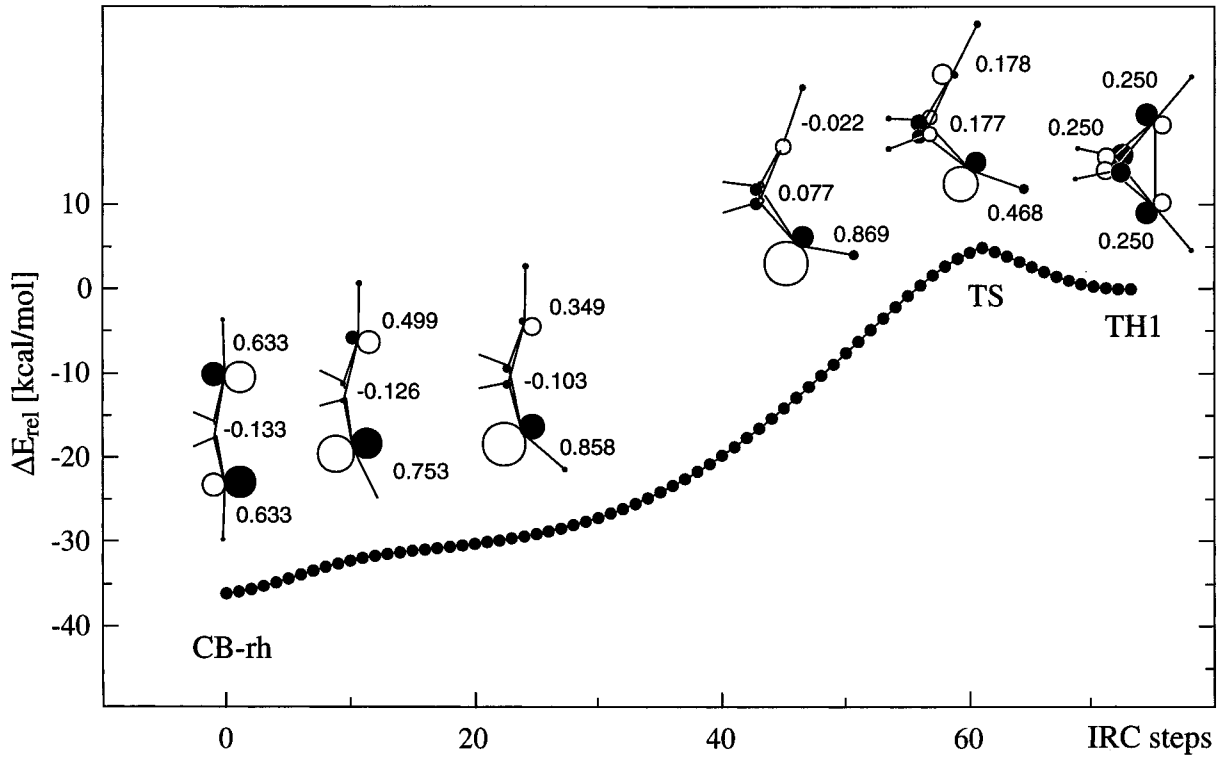

Figure 6. Results of the IRC calculation[30] for the $TH^{\bullet+} \rightarrow CB^{\bullet+}$ interconversion (ROHF/6-31G*) and change in shape of the HOMO along the reaction coordinate. The numbers indicate spin densities per C−H group from B3LYP calculations (which take spin polarization into account).

coordinate, and one expects this to be associated with some energy increase.

Before exploring this reaction, and in order to put the results for $CB^{\bullet+}$ on an equal footing with those for $TH^{\bullet+}$, we reoptimized the rectangular and rhombic structures (CB-re and CB-rh in Figure 4) corresponding to the two modes of JT stablization of $CB^{\bullet+}$ [1] at the currently used B3LYP and QCISD levels. In agreement with our previous study which was done at the RMP2 level,[1] we found both structures to be minima on the respective surfaces, but the two methods disagree on their energetic ordering. Whereas the rectangle is favored by 2.11 kcal/mol by B3LYP (1.29 kcal/mol on a ΔE_0 scale), the situation is reversed in favor of the puckered rhombus at the QCISD level by 0.76 kcal/mol (0.94 kcal/mol in ΔE_0). Single-point CCSD-(T)/cc-pVTZ calculations at the QCISD geometries predict again a small advantage for the rectangle (1.60 kcal/mol in ΔE, 1.42 in ΔE_0). All of this confirms that the bottom of the JT "sombrero" of $CB^{\bullet+}$ is essentially flat and that either structure can be considered as a target state for chemical reactions leading to this cation. In the present context, the rhombic state is more convenient, so this will be used in the following discussion.

Thus we searched for a transition state of C_s symmetry (which permits localization of spin and charge) in the vicinity of the crossing point of the $^2B_2$ surface of $CB^{\bullet+}$ and the $^2A_1$ surface of $TH^{\bullet+}$ (cf. Figure 5) and located it at all levels of calculation used in the present study (structure TS in Table 1 and Figure 4). Finally we performed an IRC calculation[30] at the ROHF/6-31G* level, starting from TS in both directions. The results of this are displayed in Figure 6 which illustrates also the change in shape of the HOMO and the spin distribution along the reaction coordinate. The strong localization of the spin expresses itself also in the pronounced pyramidalization of one C atom in the vicinity of TS. Interestingly, the maximal localization occurs not at TS but in the following downhill region of the potential energy surface leading to $CB^{\bullet+}$.

It should be noted that (at least at the ROHF level) the transition state lies slightly *higher* in energy than the (apparent) crossing point of the $^2A_1$ surface of $TH^{\bullet+}$ and the $^2B_2$ surface of $CB^{\bullet+}$. In part this is due to the fact that the two states do not really cross at this energy because their geometries are slightly different for $\Delta R = -0.38$ Å (the apparent crossing point, cf. also ref 28) and hence the "real" intersection of the two surfaces occurs at higher energy. In addition, any adiabatic transition between the two states requires further distortion to lower symmetry, possibly resulting in a further energy increase. This is in contrast to the situation which prevails in orbital-symmetry-forbidden rearrangements of closed-shell species (such as the thermal TH → CB interconversion[6]). There, an avoided crossing of surfaces usually leads to an energy *lowering* because the two *states* are of the same symmetry and can therefore experience appreciable stabilization through mixing without distortion to lower symmetry.

5. Conclusion

We have explored the potential energy surface for the Jahn−Teller (JT) distortions of $TH^{\bullet+}$ and its subsequent rearrangement to $CB^{\bullet+}$ at high levels of ab initio theory as well as by density functional methods. Thereby we found, in contrast to earlier MNDO calculations,[6] that relaxation of vertically formed $TH^{\bullet+}$ along the D_{2d} JT coordinate leads to a stable structure. Although the JT distortion represents structural progress on the reaction coordinate which connects $TH^{\bullet+}$ to $CB^{\bullet+}$, there remains a barrier of about 4 kcal/mol separating the two isomers which arises in part from the localization of the spin that is required for an adiabatic crossover from the $^2A_1$ ground-state surface of $TH^{\bullet+}$ to the $^2B_2$ surface of $CB^{\bullet+}$. This barrier should suffice to stabilize $TH^{\bullet+}$ at low temperatures and under conditions where the excess energy of about 25 kcal/mol from the vertical ionization of TH can be dissipated efficiently. In the case of the experimentally accessible tetra-*tert*-butyl derivative, a part of this energy dissipation could be "internal" such that chances of stabilizing the corresponding cation could be higher.

Acknowledgment. This work has been funded through Grant 2028-0472212.96/1 of the Swiss National Science Foundation and is part of a joint project between the University of Fribourg (Institute of Physical Chemistry) and the Academy of Sciences of the Czech Republic (J. Heyrovský Institute), respectively, under COST action D3 (Theory and Modeling of Chemical Systems and Processes) funded in Prague by the Czech Ministry of Education. We wish to thank the Swiss Center for Scientific Computing in Manno for a generous allocation of CPU time on the NEC SX3 without which the CC calculations would have been impossible to carry out.

Supporting Information Available: Full Cartesian coordinates of the structures in Figure 4 (5 pages). Consult any current masthead page for ordering or Internet access information.

References and Notes

(1) Part 1: Roeselová, M.; Bally, T.; Jungwirth, P.; Čársky, P. *Chem. Phys. Lett.* **1995**, *234*, 395.

(2) Maier, G. *Angew. Chem.* **1988**, *100*, 317; *Angew. Chem., Int. Ed. Engl.* **1988**, *27*, 309.

(3) In addition to the tetra-*tert*-butyl derivative (Maier, G.; Pfriem, S. *Angew. Chem.* **1978**, *90*, 551; *Angew. Chem., Int. Ed. Engl.* **1978**, *17*, 519), three additional derivatives have recently become available, i.e., one where a *tert*-butyl group is replaced by $SiMe_3$ (Maier, G.; Born, B. *Angew. Chem.* **1989**, *101*, 1085; *Angew. Chem., Int. Ed. Engl.* **1989**, *28*, 1050), and two where the fourth substituent is adamantyl or isopropyl (Maier, G.; Fleischer, F.; Kalinowski, H.-O. *Liebigs Ann.* **1995**, 173).

(4) Unsuccessful attempts to prepare parent TH are summarized in ref 2.

(5) Deviation from T_d to the (chiral) T symmetry was predicted (Hounshell, W. D.; Mislow, K. *Tetrahedron Lett.* **1979**, 1205) and confirmed by MNDO (Schweig, A.; Thiel, W. *J. Am. Chem. Soc.* **1979**, *101*, 4742) and may be responsible for the large vibrational ellipsoids of the methyl carbons in the crystal structure (Irngartinger, H.; Goldmann, A.; Jahn, R.; Nixdorf, M.; Rodewald, H.; Maier, G.; Malsch, K.-D.; Emrich, R. *Angew. Chem.* **1984**, *96*, 967; *Angew. Chem., Int. Ed. Engl.* **1984**, *23*, 993).

(6) Bock, H.; Roth B.; Maier, G. *Angew. Chem.* **1980**, *92*, 213; *Angew. Chem., Int. Ed. Engl.* **1980**, *19*, 209; *Chem. Ber.* **1984**, *177*, 172.

(7) Fox, M. A.; Campbell, K. A.; Hünig, S.; Berneth, H.; Maier, G.; Schneider, K.-A.; Malsch, K.-D. *J. Org. Chem.* **1982**, *47*, 3408.

(8) Maier, G.; Raug, H.; Emrich, R.; Gries, S.; Irngartinger, H. *Liebigs Ann.* **1995**, 161.

(9) Bally, T. *J. Mol. Struct. (THEOCHEM)* **1991**, *227*, 249.

(10) For previous work, see: Jungwirth, P.; Čársky, P.; Bally, T. *J. Am. Chem. Soc.* **1993**, *115*, 5776. Jungwirth, P.; Bally, T. *Ibid.* **1993**, *115*, 5783, and ref 1.

(11) Jungwirth, P.; Čársky, P.; Bally, T. *Chem. Phys. Lett.* **1992**, *195*, 371.

(12) Bersuker, I. B. *The Jahn-Teller Effect and Vibronic Interactions in Modern Chemistry*; Plenum Press: New York, 1983.

(13) Heilbronner, E.; Jones, T. B.; Krebs, A.; Maier, G.; Malsch, K.-D.; Pocklington, J.; Schmelzer, A. *J. Am. Chem. Soc.* **1980**, *102*, 564.

(14) Coffman, R. E. *J. Chem. Phys.* **1966**, *44*, 2305.

(15) This becomes evident if one transforms the equation for ϵ_1 by epressing Q_a and Q_b in polar coordinates $Q_a = \rho\cos(\phi)$ and $Q_b = \rho\sin(\phi)$. Then it simplifies to $\epsilon_1 = {}^1/_2K_E\rho^2 - \rho\sqrt{F_E{}^2+G_E{}^2\rho^2+2F_EG_E\rho\cos(3\phi)}$. For $G_E = 0$ this goes to $\epsilon_1 = {}^1/_2K_E\rho^2 - \rho|F_E|$ which is obviously independent of ϕ.

(16) This choice is not unambiguous. We could equally well take the separation of the *transition state* from the conical intersection as a third condition, and then it would be that parameter which is modeled optimally. However, it turns out that in actual fact the choice of one stationary point introduces no big errors in the opposite one.

(17) Ceulemans, A.; Beyens, D.; Vanquickenborne, L. G. *J. Am. Chem. Soc.* **1984**, *106*, 5824; Ceulemans, A.; Vanquickenborne, L. G. *Struct. Bonding* **1989**, *71*, 125.

(18) This is a combination of Becke's hybrid gradient corrected exchange functional with three parameters (Becke, A. D. *J. Chem. Phys.* **1993**, *98*, 5648), combined with the correlation functional of Lee, Yang, and Parr (Lee, C.; Yang, W.; Parr, R. G. *Phys. Rev. B* **1988**, *37*, 785). For a description of the density functionals as implemented in the Gaussian series of programs, see: Johnson, B. G.; Gill, P. M. W. L.; Pople, J. A. *J. Chem. Phys.* **1993**, *98*, 5612.

(19) (a) Ziegler, T. *Chem. Rev.* **1991**, *91*, 651. (b) Johnson, B. G.; Gill, P. M. W.; Pople, J. A. *J. Chem. Phys.* **1993**, *98*, 5612. (c) Handy, N. C.; Murray, C. W.; Amos, R. D. *J. Phys. Chem.* **1993**, *97*, 4392. (d) Stephens, B. J.; Devlin, I. J.; Chabalowsky, C. F.; Frisch, M. J. *J. Phys. Chem.* **1994**, *98*, 11623. (e) Rauhut, G.; Pulay, P. *J. Am. Chem. Soc.* **1995**, *117*, 4167; *J. Phys. Chem.* **1995**, *99*, 3093. (f) Bauschlicher, C. W.; Partridge, H. *Chem. Phys. Lett.* **1995**, *240*, 533. (g) Martin, J. M. L.; El-Yazal, J.; François, J.-P. *Chem. Phys. Lett.* **1995**, *242*, 570.

(20) See, e.g.: Baker, J.; Scheiner, A.; Andzelm, J. *Chem. Phys. Lett.* **1993**, *216*, 380. In the present case, all $\langle S^2 \rangle$ values were <0.754 except for rhombic CB (0.770) and the transisition state (0.760).

(21) Quadratic configuration interaction with single and double substitutions based on a UHF reference wave function (Pople, J. A.; Head-Gordon, M.; Rahavachari, K. *J. Chem. Phys. B* **1987**, *87*, 5968), an approximation to the CCSD method.[24]

(22) Hariharan, P. C.; Pople, J. A. *Theor. Chim. Acta* **1973**, *298*, 213.

(23) Complete Active Space SCF calculations (see, e.g.: Roos, B. In *Lecture Notes in Qauntum Chemistry*; Springer: Berlin 1992). This corresponds to a full CI calculation within a limited subset (the "active space") of valence MOs while the MO basis is simultaneously optimized for that CI by varying the AO coefficients. In the present case, the active space included four bonding and four antibonding C−C MOs.

(24) Coupled cluster calculation accounting for single and double excitations (see, e.g.: Bartlett, R. J. *J. Phys. Chem.* **1989**, *93*, 1697 and references therein) augmented by a quasi-perturbative estimate for triple excitations (Raghavachari, K.; Trucks, G. W.; Pople, J. A.; Head-Gordon, M. *Chem. Phys. Lett.* **1989**, *157*, 479). Extensive applications have shown that this method consistently yields results very close to those obtained by full configuration interaction (cf.: Lee, T. J.; Scuseria, G. E. In *Quantum Mechanical Electronic Structure Calculations with Chemical Accuracy*; Langhoff, S. R., Ed.; Kluwer: Dordrecht, 1995). Note also, that at this level, the choice of a reference SCF wave fuction (UHF or ROHF) makes no significant difference to the final results (cf. e.g.: Stanton, J. F. *J. Chem. Phys.* **1994**, *191*, 371).

(25) Dunning, T. H. *J. Chem. Phys.* **1989**, *90*, 1007.

(26) Frisch, M. J.; Trucks, G. W.; Schlegel, H. B.; Gill, P. M. W.; Johnson, B. G.; Robb, M. A.; Cheeseman, J. R.; Keith, T.; Petersson, G. A.; Montgomery, J. A.; Raghavachari, K.; Al-Laham, M. A.; Zakrzewski, V. G.; Ortiz, J. V.; Foresman, J. B.; Cioslowski, J.; Stefanov, B. B.; Nanayakkara, A.; Challacombe, M.; Peng, C. Y.; Ayala, P. Y.; Chen, W.; Wong, M. W.; Andres, J. L.; Replogle, E. S.; Gomperts, R.; Martin, R. L.; Fox, D. J.; Binkley, J. S.; DeFrees, D. J.; Baker, J.; Stewart, J. P.; Head-Gordon, M.; Gonzalez, M. C.; Pople, J. A. Gaussian, Inc.: Pittsburgh PA, 1995.

(27) The relaxation of $TH^{\bullet+}$ from the structure of neutral TH within T_d symmetry is minimal ($\Delta R < 0.01$ Å, $\Delta E < 0.3$ kcal/mol), but as the geometry optimization of the ^2E state of $TH^{\bullet+}$ is very difficult, we decided to use the structure of neutral TH for TH0.

(28) Note that in Figure 5 the crossing point of the D_{2d} curves for the $^2A_1$ and the $^2B_1$ state of $TH^{\bullet+}$ lies about 4 kcal/mol *below* the T_d conical intersection TH0. In contrast to the previous case of (planar) $CB^{\bullet+}$,[1] where symmetry requires that the crossing point of the rhombic and rectangular D_{2h} JT curves coincides with the D_{4h} conical intersection, $TH^{\bullet+}$ has an additional degree of freedom (the ratio of the lengths of the two and the four symmetry-equivalent C−C bond lengths, respectively) which differs in the two states. Therefore the crossing point of the D_{2d} curves does *not* correspond to a common geometry of both states which is attained only in TH0, the conical intersection.

(29) Bally, T.; Truttman, L.; Dai, S.; Williams, F. *J. Am. Chem. Soc.* **1995**, *117*, 7916.

(30) IRC = intrinsic reaction coordinate (see: Gonzales, C.; Schlegel, H. B. *J. Chem. Phys.* **1989**, *90*, 2154; *J. Phys. Chem.* **1990**, *94*, 5523).